AGU ADVANCING EARTH AND SPACE SCIENCE

Geophysical Research Letters

RESEARCH LETTER
10.1029/2022GL101499

Circus Tents, Convective Thresholds, and the Non-Linear Climate Response to Tropical SSTs

Andrew I. L. Williams[1], Nadir Jeevanjee[2], and Jonah Bloch-Johnson[3]

[1]Atmospheric, Oceanic and Planetary Physics, Department of Physics, University of Oxford, Oxford, UK, [2]Geophysical Fluid Dynamics Laboratory, Princeton, NJ, USA, [3]National Centre for Atmospheric Science, Reading, UK

Key Points:

- Contrary to assumptions made in previous work, we find that the climate response to tropical sea-surface temperatures is highly non-linear
- These non-linearities are most stark in the Central Pacific, and manifest even for very small perturbation magnitudes
- Non-linearity is a fundamental consequence of tropical dynamics, with important implications for prior work using linear Green's functions

Supporting Information:

Supporting Information may be found in the online version of this article.

Correspondence to:

A. I. L. Williams,
andrew.williams@physics.ox.ac.uk

Citation:

Williams, A. I. L., Jeevanjee, N., & Bloch-Johnson, J. (2023). Circus tents, convective thresholds, and the non-linear climate response to tropical SSTs. *Geophysical Research Letters*, *50*, e2022GL101499. https://doi.org/10.1029/2022GL101499

Received 3 OCT 2022
Accepted 4 FEB 2023

Author Contributions:

Conceptualization: Andrew I. L. Williams, Nadir Jeevanjee, Jonah Bloch-Johnson
Formal analysis: Andrew I. L. Williams
Methodology: Andrew I. L. Williams, Nadir Jeevanjee, Jonah Bloch-Johnson
Visualization: Andrew I. L. Williams
Writing – original draft: Andrew I. L. Williams
Writing – review & editing: Andrew I. L. Williams, Nadir Jeevanjee, Jonah Bloch-Johnson

Abstract Using model simulations, we demonstrate that the climate response to localized tropical sea surface temperature (SST) perturbations exhibits numerous non-linearities. Most pronounced is an asymmetry in the response to positive and negative SST perturbations. Additionally, we identify a "magnitude-dependence" of the response on the size of the SST perturbation. We then explain how these non-linearities arise as a robust consequence of convective quasi-equilibrium and weak (but non-zero) temperature gradients in the tropical free-troposphere, which we encapsulate in a "circus tent" model of the tropical atmosphere. These results demonstrate that the climate response to SST perturbations is fundamentally non-linear, and highlight potential deficiencies in work which has assumed linearity in the response.

Plain Language Summary Previous work has highlighted that Earth's energy balance is sensitive to the precise distribution of sea-surface temperatures (SSTs), particularly in the tropical Pacific, with important implications for inferring climate sensitivity from the historical record. To quantify this "SST pattern effect," many studies have adopted a linear framework where the climate response to an SST anomaly is assumed to be a linear function of the sign and size of the anomaly. Here, we show that this assumption is not applicable in many parts of the tropics, particularly the Central Pacific. We classify these non-linearities into two classes and explain why they arise in terms of simple tropical dynamics. To summarize our findings we use a conceptual model of the tropical atmosphere which we term the "circus tent" model, which represents the dynamics behind these non-linearities in an intuitive way. Our work suggests that previous work which has assumed linearity in the climate response to tropical SSTs may be suffering from compensating biases in their response.

1. Introduction

The spatial pattern of tropical sea-surface temperatures (SSTs) exerts a strong influence on Earth's climate, particularly on the radiative fluxes at the top-of-atmosphere (TOA). First recognized in the context of the El Niño–Southern Oscillation (ENSO) (Bjerknes, 1969; Park & Leovy, 2004; Trenberth et al., 2002), in recent years, this dependence of TOA fluxes on the spatial pattern of sea surface temperature (SST) changes has been re-framed into the broader concept of the "SST pattern effect" (Stevens et al., 2016). The SST pattern effect has received considerable attention within the community due to its implications for reconciling the anomalously low climate sensitivity inferred from historical energy budget constraints (Knutti et al., 2017; Otto et al., 2013) with the climate sensitivity calculated by equilibrating climate models (Andrews et al., 2018; Rugenstein et al., 2020).

Both modeling (Andrews & Webb, 2018; Dong et al., 2019; Zhou et al., 2016) and observational (Fueglistaler, 2019; Mackie et al., 2021) studies have suggested that the primary mechanism mediating the SST pattern effect is its influence on low clouds in regions of climatological subsidence, and such explanations typically proceed as follows:

- Regions with a high climatological low-cloud amount are generally associated with cold SSTs and a strong inversion (Wood & Bretherton, 2006), thus when SSTs in these regions are warmed the inversion weakens and there is a decrease in low-level cloudiness. This leads to a positive shortwave TOA (SW_{TOA}) anomaly through reduced low-level reflection of incoming solar radiation. The reverse-argument also holds, namely that isolated cooling in these regions strengthens the inversion and increases low-level cloudiness. We term this the "local stability-inversion" mechanism.
- On the other hand, warming in regions of deep convection is communicated vertically throughout the free-troposphere by deep convection (Y. Zhang & Fueglistaler, 2020) and then horizontally across the tropics through the action of gravity waves (Bretherton & Smolarkiewicz, 1989; Charney, 1963; Neelin &

Held, 1987; Pierrehumbert, 1995). This causes a remote warming of the free-troposphere over the aforementioned low-cloud regions which again strengthens the inversion and increases the low-cloud amount (Andrews & Webb, 2018). We term this the "non-local stability-inversion" mechanism.

Warming of the free-troposphere has also been shown to affect the TOA flux response through the lapse-rate feedback (Andrews & Webb, 2018; Ceppi & Gregory, 2017), in addition to the cloud feedbacks which we highlight here. However, when a relative humidity-based decomposition (Ceppi & Gregory, 2017; Held & Shell, 2012) is used (which accounts for the partial cancellation between lapse-rate and water-vapor feedbacks (Dong et al., 2019)), the lapse-rate feedback has been found to be smaller in magnitude than the cloud radiative feedback.

This explanation has gained significant traction in explaining the SST pattern effect, to the point of appearing in the latest IPCC report (Forster et al., 2021), and is qualitatively supported by analysis of coupled climate model experiments (Ceppi & Gregory, 2017). To put the SST pattern effect on a more quantitative footing some studies have framed the problem in terms of Green's functions (Baker et al., 2019; Dong et al., 2019; Li & Forest, 2014; Zhou et al., 2017) by assuming there exists some operator, $\mathcal{G}$, which maps the spatial pattern of SST anomalies onto TOA anomalies. In this framework, $\mathcal{G}$ can be estimated using ensembles of isolated "SST patch" experiments in an atmosphere only model and then used to reconstruct the TOA response to arbitrary SST patterns. Although this is an appealing concept, a potential issue is that the Green's function approach is fundamentally linear (Riley et al., 1999) and requires assuming that the TOA response is linear with respect to the sign and magnitude of the imposed SST anomaly, and also that SST anomalies in different regions *combine* linearly. Previous studies have made these assumptions (Baker et al., 2019; Barsugli & Sardeshmukh, 2002; Dong et al., 2019; Li & Forest, 2014; Zhou et al., 2017), but given the well-appreciated "threshold" behavior of deep convection (Emanuel, 2007; Johnson & Xie, 2010; I. N. Williams & Pierrehumbert, 2017; Xie et al., 2010; C. Zhang, 1993; Y. Zhang & Fueglistaler, 2020) (see Section 2), along with the observed asymmetry in the atmospheric response to positive and negative ENSO phases (Hoerling et al., 1997, 2001; Johnson & Kosaka, 2016), it seems likely that the linear assumption is not valid.

As such, our goal in this paper is to evaluate the linear assumptions made by previous studies, and to explain why non-linearities arise from the perspective of basic tropical dynamics. We begin by reviewing the theoretical basis for the "threshold" behavior of deep convection, and then use atmosphere-only model experiments to show that the TOA response to isolated SST anomalies is in fact non-linear. To explain these findings we then introduce a simple conceptual picture of the tropical atmosphere's response to SST perturbations, which we term the "circus tent" model, which builds on previous work in the tropical dynamics community. Finally, we show that in regions of deep convection the change in TOA flux associated with a positive SST anomaly can be explained simply by the change in low-level moist static energy and examine to what extent these changes are predictable purely from the SST changes.

2. Theory

To link the dynamics of deep convection to the free-tropospheric temperature profile, we will frequently make use of the moist static energy in this paper, defined as:

$$h = c_p T + L_v q + g z, \tag{1}$$

where c_p is the heat capacity of dry air, T is temperature, g is gravitational acceleration, z is height, L_v is the latent heat of vapourization of water, and q is the water vapor specific humidity. The moist static energy is useful as it is approximately conserved under moist, adiabatic motion.

A central pillar of our understanding of the tropical atmosphere is the assumption of convective quasi-equilibrium (Betts, 1982; Emanuel, 2007; Raymond, 1995), which holds that deep convection relaxes the free-tropospheric temperature profile to a moist adiabat set by the properties of the subcloud layer. As a moist adiabat is associated with constant saturation moist static energy, this is another way of saying that in regions of deep convection the saturation moist static energy (i.e., Equation 1 but with q replaced by its value at saturation, q^*) of the free-troposphere, h^*_{FT}, should approximately equal the moist static energy of the subcloud layer, h_0. Note also that because ascending parcels mix with relatively dry air from the environment through entrainment (Singh & O'Gorman, 2013) regions of convection tend to be associated with a h_0 slightly in excess of h^*_{FT} (e.g., Figure 2a), but this does not strongly affect our results.

As mentioned before, gravity waves are efficient at communicating this local temperature profile imposed by convection (or equivalently, h^* profile) across the tropics. This means that deep convection in one region can communicate

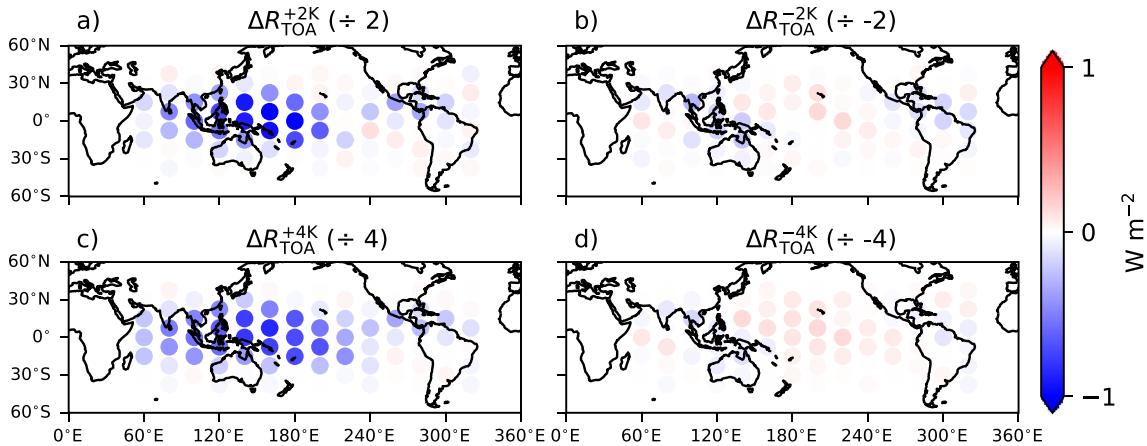

Figure 1. Change in global-mean top-of-atmosphere flux (ΔR_{TOA}) associated with each of the sea surface temperature perturbation experiments. (a) Changes for +2K patches, divided by 2. (b) Changes for −2K patches, divided by −2. Panels (c, d) as in panels (a, b) but divided by ±4.

high values of h^*_{FT} across the tropical free-troposphere, establishing a "convective threshold" which inhibits the formation of deep convection if the subcloud h_0 is not sufficient in these regions to overcome the imposed h^*_{FT}.

Using this observation, we follow previous work (e.g., I. N. Williams & Pierrehumbert, 2017) in defining a "convective instability index," $h_0 - h^*_{500}$, (taking the 500 hPa level to be representative of the free-troposphere). In regions unstable to deep convection, we expect this quantity to be positive, whereas in regions stable against deep convection (e.g., subsiding regions) we expect this to be negative and to act as a measure of the inversion strength (similar to Wood and Bretherton (2006), but also accounting for moisture differences as in Koshiro et al. (2022)).

A further simplifying assumption which is frequently made assumption is that h^*_{500} is uniform across the free-troposphere (the "weak temperature gradient" assumption, WTG), which allows one to replace h^*_{500} with its tropical average value (establishing a single value for the convective threshold). However, as we will show later, this assumption is misleading in the context of the pattern effect, where warming-induced changes in h^*_{500} are comparable to the spatial variations in baseline h^*_{500} arising from non-zero zonal temperature gradients (Bao & Stevens, 2021; Bao et al., 2022; Fueglistaler et al., 2009). This means that there are actually a spectrum of values for the convective threshold, depending on the local value of h^*_{500}, and to fully understand the pattern effect we cannot assume a single value for h^*_{500}.

3. Methods

We performed a series of atmosphere-only simulations using the ICOsahedral Non-hydrostatic general circulation model. The model is run on a triangular grid, at R_2B_4 specification, corresponding to an approximately uniform grid-spacing of 160 km on a Cartesian grid. The model uses a terrain-following vertical sigma-height grid with 47 levels between the surface and the model top at 83 km. Radiation is parameterized using PSrad scheme (Pincus & Stevens, 2013), and other parameterizations include a bulk mass-flux convection scheme (Tiedtke, 1989), a relative-humidity based cloud cover scheme (Sundqvist et al., 1989) and a single-moment microphysics scheme (Baldauf et al., 2011). In our experiments all greenhouse gases and ozone are fixed at their 1979 levels (A. I. L. Williams et al., 2022).

The control simulation was run for 20 years with a prescribed monthly climatology of SSTs and sea-ice concentrations derived from the Atmospheric Model Intercomparison Project (Neale & Hoskins, 2000) boundary conditions over 1979–2016. Then additional simulations were conducted for 10 years each with an additional "cosine patch" SST perturbation (following Barsugli and Sardeshmukh (2002)) covering different locations throughout the tropics (perturbation centers correspond to the centers of each of the circles in Figure 1 and an example SST perturbation is shown in Figure S1b in Supporting Information S1). For all simulations, we discard the first year as spin-up and conduct analysis using time-averages over the rest of the simulation period.

The subcloud moist static energy (h_0) was calculated using values at the lowest model level, and the free-tropospheric saturation moist static energy was approximated by its value at 500 hPa $\left(h^*_{500}\right)$. Our conclusions are insensitive to

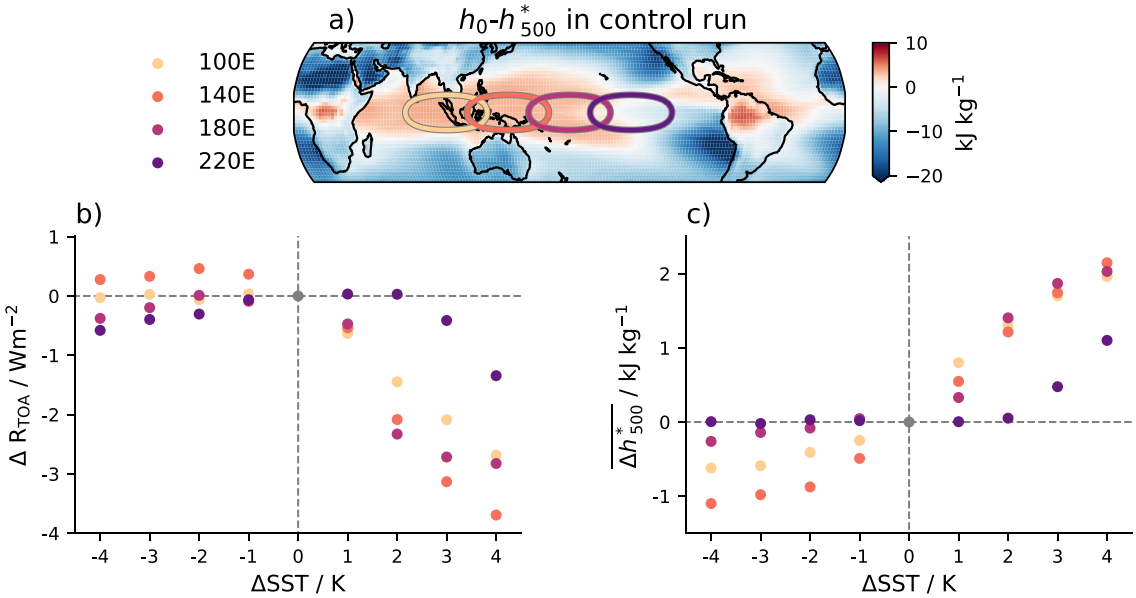

Figure 2. (a) The half-amplitude contours of the four locations of the different equatorial sensitivity experiments are overlaid on top of the "convective instability" parameter (h_0-h^*_{500}) in the control run. (b) The changes in global-mean R_{TOA} for each of the sensitivity experiments at ±1K, ±2K, ±3K, and ±4K. (c) as in (b) but showing the change in tropical-average h^*_{500}, denoted $\overline{\Delta h^*_{500}}$. To account for the varying amounts of land in different patches, in panels (b and c) the ΔR_{TOA} and $\overline{\Delta h^*_{500}}$ have been divided by the ΔSST weighted land-fraction before plotting.

the precise choice of levels, and similar results were obtained when either calculating the subcloud moist static energy as the average moist static energy over the lowest 1 km (lowest 5 model levels) or calculating the saturation free-tropospheric moist static energy as a bulk average over 700 hPa-300 hPa. Also note that because h_0 is defined at a given height level, warming-induced changes in h_0 are only due to changes in temperature and humidity at that level.

We also define two averaging operators which make the presentation clearer. An overbar $\overline{(\cdot)}$ indicates an average over tropical latitudes (±30°), and angle brackets $\langle(\cdot)\rangle$ indicates a *local* "patch-average" over the region covered by the SST patch perturbation in that experiment (i.e., over ocean grid-points with |ΔSST| > 0). For example, $\langle\Delta h_0\rangle$ is the change in low-level moist static energy in a particular patch experiment, averaged over all *ocean* grid-points where |ΔSST| > 0 (see Figure S1b in Supporting Information S1 for an example). Similarly, $\langle\Delta h^*_{500}\rangle$ is the change in saturation free-tropospheric moist static energy at 500 hPa, averaged over the underlying grid-points which are ocean and have |ΔSST| > 0. All spatial averages include area-weighting.

4. Results

4.1. Non-Linear TOA Response to Tropical SSTs

In Figure 1 we plot the globally averaged change in net TOA radiation (ΔR_{TOA}) for each of the tropical SST perturbation experiments, relative to the control. In agreement with previous work Figures 1a and 1c shows that SST warming in the Western tropical Pacific (a region of climatological deep convection), is associated with strong, negative changes in the global-mean R_{TOA} flux via the "non-local stability-inversion" mechanism (Dong et al., 2019; Zhou et al., 2017). The results are similar if we focus on the SW (Figure S2 in Supporting Information S1). Additionally, in subsiding regions the ΔR_{TOA} is slightly positive for the +2K and +4K patches, indicating the "local stability-inversion" mechanism is at work. However, if we compare these results to the cooling patch experiments in Figures 1b and 1d we can see there is a marked asymmetry in the ΔR_{TOA} response between the warming and cooling experiments (note that we have normalized all experiments by the magnitude and sign of the SST perturbations, so if the system was linear all of the panels in Figure 1 would be identical). Notably, whereas warming in convective regions generates a strongly negative ΔR_{TOA}, cooling in convective regions has a comparatively small influence on the R_{TOA} (Figure 1b). Additionally, while the ΔR_{TOA} increases approximately linearly with SST warming (i.e., the values are similar in Figures 1a and 1c), for SST cooling in convective regions the R_{TOA} does not change linearly (i.e., the negative values over the West Pacific are smaller in Figure 1d

than Figure 1c). The spatial patterns of ΔR_{TOA} are presented in Figure S3 in Supporting Information S1 for a representative patch in the West Pacific and confirm these findings.

Alongside this "asymmetry" in the ΔR_{TOA} between warming and cooling patches, there is also another, more subtle, non-linearity that appears in our experiments. To spot this, compare the ΔR_{TOA} responses in the Central Pacific between the +2K experiments in Figure 1a and +4K experiments in Figure 1c. Although the ΔR_{TOA}^{+4K} response is generally around twice the ΔR_{TOA}^{+2K} response (note that the values in Figures 1a and 1c are divided by 2 to make them comparable to the +2K experiments), in the weakly stable regions of the Central Pacific there are numerous experiments where the ΔR_{TOA} either changes sign or becomes much more negative at +4K compared to +2K. We term this the "magnitude-dependence" of the SST pattern effect, to convey that the strongly negative ΔR_{TOA} only kicks in for ΔSST above a certain magnitude in these moderately stable regions.

To dig into this more, we have performed additional simulations at ±1K and ±3K for a subset of four patches along the equatorial Pacific (Figure 2a). As indicated by the shading in the background of Figure 2a, these four patches cover distinct convective regimes (as $h_0 - h^*_{500}$ is a measure of convective instability, see Theory). The patches at 100E and 140E are in strongly convective regions (where h_0-$h^*_{500} > 0$), whereas the patch at 220E is in a region which is stable to deep convection (where h_0-$h^*_{500} < 0$) and the patch at 180E is in a transition region. In Figure 2b we have plotted the global-mean ΔR_{TOA} for each of the four patches at $\Delta SST = \pm 1K, \pm 2K, \pm 3K$, and ±4K. Again, the asymmetry in the TOA response between positive and negative perturbations is evident. Taking the 140E patch as an example, positive ΔSST perturbations induce a negative ΔR_{TOA} which scales quasi-linearly with the ΔSST magnitude, but for negative ΔSST the TOA response quickly saturates. It is a similar story for the 100E patch, but the signal is weaker for negative ΔSST, however if we subset the TOA response only over subsiding regions we recover the same behavior (Figure S4 in Supporting Information S1).

This asymmetry is also evident in how the ΔSST perturbations impact on the tropical-average saturation moist static energy, $\overline{h^*_{500}}$ (Figure 2c), which makes sense as a higher $\overline{h^*_{500}}$ indicates a warmer and more stable free-troposphere which tends to increase the inversion over low-cloud regions. Looking again at the 140E patch confirms our suspicion that greater $\overline{\Delta h^*_{500}}$ is associated with greater ΔR_{TOA} for positive values of ΔSST. Conversely, for negative ΔSST there is an initial decrease in $\overline{h^*_{500}}$, which quickly saturates. For other "convective" patch at 100E it is a similar story. It is also worth noting here that in non-convective regions, negative ΔSST also causes a negative ΔR_{TOA}, which strengthens with larger ΔSST (Figure 2b), even without impacting on the $\overline{h^*_{500}}$ (Figure 2c).

Previously we also noted a "magnitude dependence" of ΔR_{TOA} on the magnitude of positive ΔSST changes in moderately stable regions (Figures 1a and 1c) and this is again present in Figure 2. Looking at the 220E patch results in Figure 2b, we can see that the sharp decrease in R_{TOA} does not occur until $\Delta SST \gtrsim 2K$, whereas for the other patches the quasi-linear decrease occurs for all $\Delta SST > 0K$. A similar picture exists for the $\overline{\Delta h^*_{500}}$, which is unaffected until $\Delta SST \gtrsim 2K$ for the 220E patch (Figure 2c).

4.2. A Conceptual Model for the Non-Linear Response

To understand this behavior, it is helpful to introduce a conceptual picture which builds on our earlier discussion of convective quasi-equilibrium and weak (but non-zero) temperature gradients in the free-troposphere. We call this the "circus tent" model and it is sketched in Figure 3a. This conceptual model was originally suggested by Isaac Held in a 2011 blog post entitled "Atlantic Hurricanes and Differential Tropical Warming." In this model, the temperature of the tropical free-troposphere (or equivalently, its h^*) can be thought of as being a tight fabric supported by "convective tent poles" of different "heights" corresponding to their subcloud h_0. Where there is deep convection, convective quasi-equilibrium ensures the height of the fabric $\left(h^*_{500}\right)$ is roughly equal to h_0, and as one moves away from the convective center the h^*_{500} profile relaxes somewhat until it comes under the influence of a different tent pole. The "tightness" of the fabric is related to the efficient homogenization of h^* anomalies by gravity waves, and the pattern of Δh^*_{500} appears to be related to the Matsuno-Gill response to tropical heating (e.g., Figure 1 of Gill (1980)), with an equatorially confined lobe extending to the East and two off-equatorial maxima slightly to the West of the heating. This pattern can be seen in our maps of Δh^*_{500} (Figure S5 in Supporting Information S1).

Using this model we can now understand the impact of warming and cooling in convective regions we saw in Figure 2. The case of positive ΔSST in convective regions is sketched in Figure 3b. In this case, because the

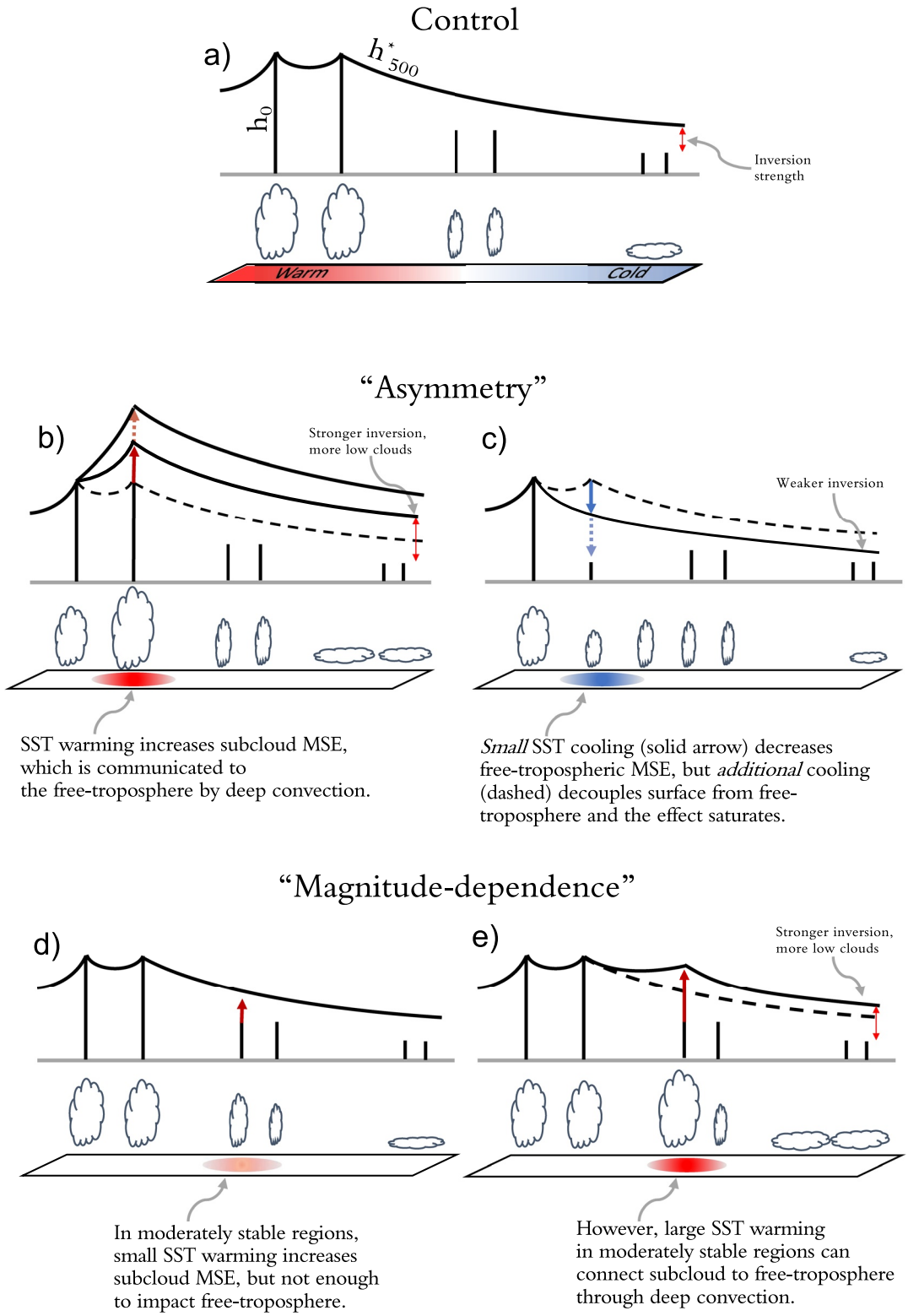

Figure 3. Schematic representation of the processes controlling the non-linear top-of-atmosphere response to sea surface temperature (SST) perturbations in different convective regimes. (a) Illustrates the "circus tent" model of the tropical atmosphere in the presence of an SST gradient, where deep convection occurs over the warmest SSTs with highest h_0 and is able to perturb the free-tropospheric temperature structure (as measured by h^*_{500}). (b, c) Conceptually illustrate how a tropical circus tent responds "asymmetrically" to warming and cooling in convective regions. (d, e) Illustrate how a tropical circus tent responds non-linearly with respect to the magnitude of the SST perturbation in moderately stable regions.

region is already convecting, we are increasing the height of a tent pole which is already "in contact" with the tent fabric, which raises the h^*_{500} throughout the free-troposphere, including over regions of low-clouds where it strengthens the inversion. Because the tent fabric is tight, this also explains why the changes in h^*_{500} and R_{TOA} are approximately linear (Figure 3b). On the other hand, Figure 3c illustrates how for negative ΔSST in convective regions the tent pole may be lowered sufficiently to lose contact with the fabric. At this point, further decreases in SST are not communicated to the free-troposphere, which explains the "saturation" of $\overline{\Delta h^*_{500}}$ and ΔR_{TOA} at negative ΔSST (Figure 2b, Figures S4–S6 in Supporting Information S1). Additionally, for non-convective regions we previously noted that negative ΔSST causes a negative ΔR_{TOA} even without changing the tropical-average h^*_{500}. To understand this, we note that non-convective regions do not "make contact" with the tent fabric, and that the difference between the height of the tent pole and the overlying fabric in this case $\left(h_0 - h^*_{500}\right)$ is a measure of inversion strength. Hence, negative ΔSST in non-convective regions perturbs R_{TOA} not by altering h^*_{500}, but by *lowering* the local values of h_0 through cooling the surface. This increases the inversion strength over this region and locally increases low-cloud coverage, leading to a negative ΔR_{TOA}.

The circus tent model of the tropics is also useful for understanding the "magnitude dependence" we have noted earlier, where even for positive ΔSST, the relationship between ΔSST and $\overline{\Delta h^*_{500}}$ or ΔR_{TOA} can be highly non-linear. This phenomena is most pronounced in moderately stable regions such as the Central Pacific, which correspond to the middle tent poles in Figure 3a which are not quite tall enough to make contact with the h^*_{500} fabric (i.e., they sit below the local convective threshold). In this situation, small SST warming raises the subcloud h_0, but may not raise it sufficiently to overcome the convective threshold and make contact with the tent fabric (Figure 3d). For the SST warming to be able to substantially alter the $\overline{\Delta h^*_{500}}$ or ΔR_{TOA}, it must be strong enough to raise this tent pole (increase the h_0) enough to make contact with and subsequently raise the height of the tent fabric, as in Figure 3e. When this condition is met, the local increase in h^*_{500} results in a stronger inversion over low-cloud regions due to the tightness of the fabric. This explains the sudden decrease in ΔR_{TOA} for the 220E patch at ΔSST > 2K.

4.3. A Linear Model for the TOA Response to SST Warming in Convective Regions

Given the non-linearities we have highlighted in the previous section, a natural question is: "Why do previous Green's function methods work at all?." One possibility is that the regions of strongest sensitivity in Green's function studies tend to be strongly convective, such as the West Pacific (Dong et al., 2019). Our own analysis shows that the relationship between ΔR_{TOA} and ΔSST is reasonably linear in convective regions (e.g., compare Figures 2b and 2c), and in this section we explore this link in more detail using the +2K and +4K experiments from Figure 1. To do this, in Figure 4a we first plot the change in patch-averaged h_0 against the patch-averaged changes in h^*_{500} for each of +2K and +4K experiments from Figure 1 which are deemed to be "convective" (i.e., if $\langle h_0 \rangle > \left\langle h^*_{500} \right\rangle$ either in the control run or in the perturbed run). The results of Figure 4a act as a test of the convective quasi-equilibrium hypothesis mentioned earlier, and confirms that changes in subcloud h_0 are efficiently transported into the local free-troposphere in regions of deep convection. Next, in Figure 4b we check to what extent these local changes in h^*_{500} relate to broader changes across the tropics. In the limit of zero horizontal temperature gradients (perfect WTG) the points in Figure 4b would lie on the one-to-one line (because any localized variations in h^*_{500} would be communicated perfectly across the tropics), but we actually find that they lie on a line of constant, but shallower, slope (gradient of about 1/3). The shallow slope indicates that the changes in h^*_{500} are not spread uniformly across the tropics (motivating our conceptual model which includes horizontal h^* gradients), and the fact that the slope is constant with increasing local forcing indicates that there is no "state-dependence" in the relationship between local and tropical-average changes in h^*_{500}. To confirm the role the changes in h^*_{500} play in the "non-local stability-inversion" mechanism, in Figure 4c we scatter the changes in $\overline{\Delta h^*_{500}}$ against ΔR_{TOA} and the strong linear relationship indicates that larger changes in free-tropospheric temperature do indeed alter the inversion strength and TOA radiation. Taken together, these results suggest that ΔR_{TOA} should be linearly related to the $\langle \Delta h_0 \rangle$ in regions of deep convection, which we find holds reasonably well in our experiments (Figure 4d).

Since local $\langle \Delta h_0 \rangle$ accounts for much of the scatter in ΔR_{TOA} for positive ΔSST in convecting regions (Figure 4d), a natural question is: can we relate $\langle \Delta h_0 \rangle$ to the ΔSST perturbation more directly? As we defined the subcloud moist static energy at a given geopotential height, we can write $\langle \Delta h_0 \rangle$ as:

$$\langle \Delta h_0 \rangle = \langle c_p \Delta T_0 + L_v \Delta q_0 \rangle.$$

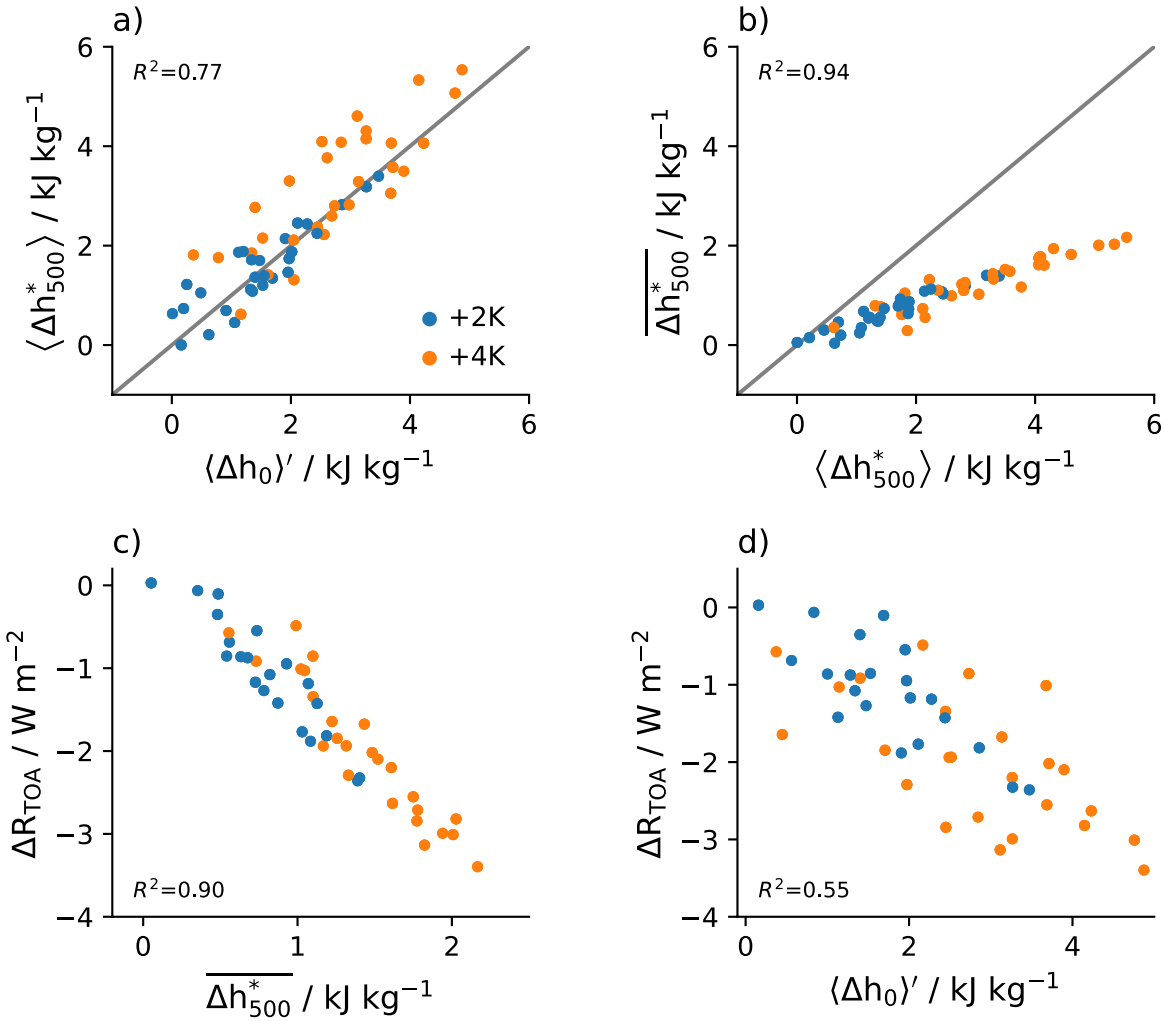

Figure 4. Evaluating the canonical model of the sea surface temperature pattern effect for warming in convective regions. (a) Shows a scatter plot of $\langle \Delta h_0 \rangle'$ versus $\langle \Delta h_{500}^* \rangle$, as a test of convective quasi-equilibrium. $\langle \Delta h_0 \rangle'$ is equal to $\langle \Delta h_0 \rangle$ except for if that local patch region does not "convect" in the control climate (i.e., $\langle h_0 \rangle < \langle h_{500}^* \rangle$), in which case we subtract the absolute value of $\langle h_0 - h_{500}^* \rangle$ from the control run to adjust for the fact that the tent fabric only "feels" the amount by which the convective threshold is exceeded. (b) shows a scatter plot of $\langle \Delta h_{500}^* \rangle$ versus $\overline{\Delta h_{500}^*}$, as a test of weak temperature gradient. (c) Shows $\overline{\Delta h_{500}^*}$ versus the global-mean ΔR_{TOA}, with the strong correlation indicating support for the "non-local stability-inversion" mechanism. Finally, (d) shows a scatter plot of the global-mean ΔR_{TOA} versus $\langle \Delta h_0 \rangle'$. Numbers indicate the Pearson coefficient of determination, R^2.

Writing $q_0 = \mathrm{RH}_0\, q_0^*$ and linearizing, we can further approximate this as:

$$\langle \Delta h_0 \rangle \approx \left\langle \left(c_p + L_v \mathrm{RH}_0 \frac{dq_0^*}{dT} \right) \Delta T_0 + L_v q_0^* \Delta \mathrm{RH}_0 \right\rangle.$$

If we also assume Clausius-Clapeyron scaling of q_0^* $\left(\text{i.e., } \frac{dq_0^*}{dT} = \frac{L_v q_0^*}{R_v T^2}\right)$, we arrive at:

$$\langle \Delta h_0 \rangle \approx \left\langle \left(c_p + \frac{\mathrm{RH}_0 L_v^2}{R_v T_0^2} q_0^* \right) \Delta T_0 + L_v q_0^* \Delta \mathrm{RH}_0 \right\rangle. \quad (2)$$

In Figure 5a, we show that Equation 2 can capture most of the variations in $\langle \Delta h_0 \rangle$ across the SST patch experiments (±2K and ±4K) conducted for Figure 1, although there are slight errors at large, positive ΔSST which we think are because we only use a first-order Taylor expansion of $\frac{dq_0^*}{dT}$ in deriving Equation 2. Next, if we assume the surface temperature is perfectly communicated across the sub-cloud layer, we can replace T_0 = SST, which also reproduces the modeled $\langle \Delta h_0 \rangle$ well (Figure 5b), with a slight overestimate at higher $\langle \Delta h_0 \rangle$. We get similar

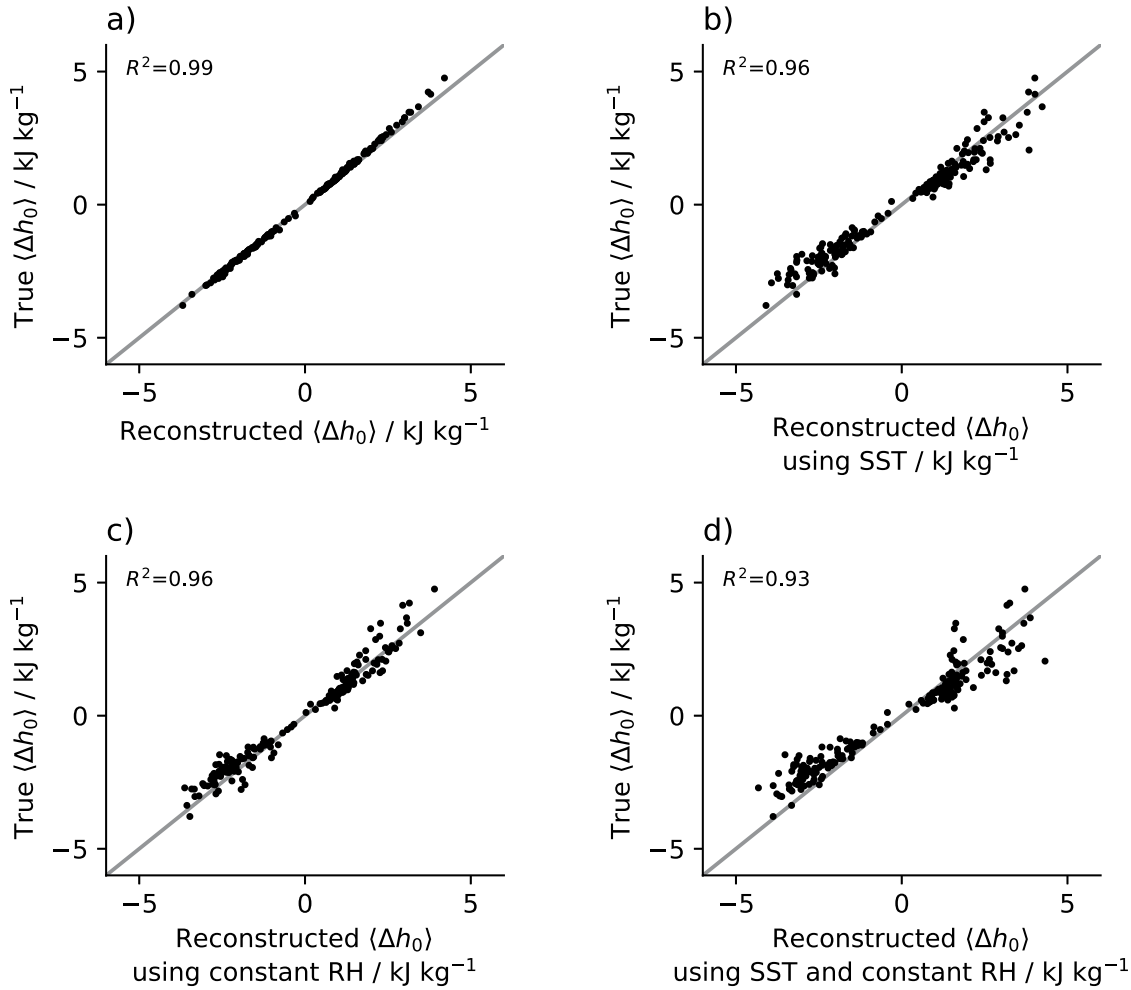

Figure 5. Estimating the true $\langle \Delta h_0 \rangle$ in each of the ±2K and ±4K sea surface temperature patch experiments from Figure 1: (a) Equation 2. (b) Equation 2 with ΔT_0 replaced by ΔSST. (c) Equation 2 with ΔRH = 0. (d) Equation 2 after making both approximations. Numbers indicate the Pearson coefficient of determination, R^2.

levels of skill if we assume constant relative humidity but include ΔT_0 (Figure 5c). This purely "thermodynamic" scaling also becomes less accurate at strong, positive ΔSST, possibly because of changes in moisture convergence. Finally, if we combine both of these approximations (ΔRH = 0 and T_0 = SST in Equation 2) we can still reconstruct changes in subcloud h_0 reasonably well (Figure 5d), even though we are only using information about the SST distribution. This provides support for work which has used SST as a proxy for changes in h_0, however for +4K perturbations we only achieve $R^2 = 0.49$ in this case, which suggests caution should be taken when using SST as a proxy for subcloud MSE at large, positive ΔSST.

5. Discussion and Conclusions

In this work we have shown that the climate response to isolated tropical SST perturbations exhibits strong non-linearities with respect to their sign, magnitude and location. We argue that these non-linearities arise primarily due to the fact that identical SST perturbations do not necessarily perturb the saturation moist static energy of the tropical free-troposphere equally, which is important for setting the inversion strength over low-cloud regions. For example, in moderately stable regions such as the Central Pacific negative SST anomalies have little impact on the global-mean TOA radiation or tropical h^*_{500}, and positive SST anomalies only have a strong effect when the ΔSST magnitude exceeds a certain value determined by the local convective threshold.

To understand these results, we have introduced the "circus tent" model of the tropical atmosphere, which brings together the twin pillars of convective quasi-equilibrium and weak (but non-zero) temperature gradients in the

tropical free-troposphere. In this model, local SST perturbations only alter the h^*_{500} if the subcloud h_0 exceeds a local "convective threshold," and then proceed to perturb the h^*_{500} quasi-linearly for positive perturbations. Negative ΔSST perturbations in convective regions can also decrease the h^*_{500} (Figure 2c), generating positive ΔR_{TOA} as a result of low-cloud changes. However, the effect saturates for sufficiently negative ΔSST because eventually the subcloud layer becomes decoupled from the free-troposphere (Figures 2b and 3c). These concepts are understood implicitly in the tropical dynamics community (Flannaghan et al., 2014; Fueglistaler et al., 2009, 2015; Zhao et al., 2009), but to our knowledge this is the first time they have been *explicitly* invoked to understand the pattern effect.

Our work has implications for studies which construct SST Green's functions by demonstrating that the TOA response is not always linear in ΔSST, even for a given sign, and that the character of the non-linearity varies depending on the convective regime being perturbed. Preliminary work as part of the Green's Function Model Intercomparison Project (GFMIP, Bloch-Johnson et al. (2023)) has also demonstrated similar non-linearities in five other GCMs, suggesting our results are not model-specific (B. Zhang et al., 2022). This does not mean the Green's function approach is without merit, but suggests that future work should focus on mapping the TOA response across multiple ΔSST values for each location and understanding the responses in isolation before combining them so as to minimize the risk of introducing compensating errors. This is currently being undertaken in a multi-model context as part of the GFMIP project (Bloch-Johnson et al., 2023). A particular focus of future work should be on understanding how SST perturbations alter the distribution of subcloud moist static energy, particular over the perturbed region, and understanding what factors set the shape of the tropical "circus tent" and its response to forcing.

It is also interesting to note that our patch experiments generate changes in the ascending area of the tropics, with warming in convective regions generally causing a decrease in the tropical ascent fraction (Figure S7b in Supporting Information S1) (Jenney et al., 2020). These changes in the ascent fraction are not necessary to explain the non-linearities we identify here (Figure S4 in Supporting Information S1), nor do they track ΔR_{TOA} in a simple way (Figure S7 in Supporting Information S1). However, changes in the ascent fraction likely enhance the low-cloud responses we identify. Understanding the response of ascent area to warming and its consistency across models is thus a fruitful avenue for future work.

Finally, although our work has focused on the climate response to *isolated* SST perturbations, the "circus tent" framework we propose also predicts that the response to SST perturbations need not *combine* linearly either (see schematic in Figure S8 in Supporting Information S1), which is another key assumption of Green's function reconstructions (e.g., Dong et al., 2019; B. Zhang et al., 2022). While Dong et al. (2019) showed that the TOA responses combined linearly when simultaneously warming the Eastern and Western tropical Pacific, our results (Figure S9 in Supporting Information S1) suggest this is a fortuitous outcome of warming one region already "in contact" with the tent fabric, and another which sits well-below it (Figure 3a, Figures S8 and S9 in Supporting Information S1). Generally our results suggest that positive SST patches in convective or marginally stable regions have a weaker impact on free-tropospheric h^* when applied simultaneously than when considering a linear sum of the individual patches. In other words, the impact of positive SST anomalies is "less than or equal to the sum of its parts." On the other hand, our framework predicts that simultaneously *cooling* multiple convective regions yields a response which is "greater than or equal to the sum of its parts." Future work could build on these results by mapping this non-additivity across regions and by applying these results to understand the response of climate to uniform warming, a problem which Green's function approaches generally struggle with (Dong et al., 2019; B. Zhang et al., 2022).

Acknowledgments
A.I.L. Williams acknowledges funding from the Natural Environment Research Council, Oxford DTP, Award NE/S007474/1 and thanks Jiawei Bao and Duncan Watson-Parris for helpful discussions. J. Bloch-Johnson acknowledges funding from the European Research Council (ERC) under the European Union's Horizon 2020 research and innovation programme (Grant 786427, project "Couplet"). We are thankful to the organizers and participants of the CLIVAR Pattern Effect workshop for creating a stimulating environment which helped to focus this work. Further thanks to Tristan Abbott, Bosong Zhang, and two anonymous reviewers for helpful feedback which improved the manuscript.

Data Availability Statement

Data from this study is available at https://doi.org/10.5281/zenodo.7621085.

References

Andrews, T., Gregory, J. M., Paynter, D., Silvers, L. G., Zhou, C., Mauritsen, T., et al. (2018). Accounting for changing temperature patterns increases historical estimates of climate sensitivity. *Geophysical Research Letters*, *45*(16), 8490–8499. https://doi.org/10.1029/2018gl078887

Andrews, T., & Webb, M. J. (2018). The dependence of global cloud and lapse rate feedbacks on the spatial structure of tropical Pacific warming. *Journal of Climate*, *31*(2), 641–654. https://doi.org/10.1175/jcli-d-17-0087.1

Baker, H. S., Woollings, T., Forest, C. E., & Allen, M. R. (2019). The linear sensitivity of the north Atlantic oscillation and eddy-driven jet to SSTs. *Journal of Climate*, *32*(19), 6491–6511. https://doi.org/10.1175/jcli-d-19-0038.1

Baldauf, M., Seifert, A., Förstner, J., Majewski, D., Raschendorfer, M., & Reinhardt, T. (2011). Operational convective-scale numerical weather prediction with the COSMO model: Description and sensitivities. *Monthly Weather Review*, *139*(12), 3887–3905. https://doi.org/10.1175/mwr-d-10-05013.1

Bao, J., Dixit, V., & Sherwood, S. C. (2022). Zonal temperature gradients in the tropical free troposphere. *Journal of Climate*, *35*(24), 1–28. https://doi.org/10.1175/jcli-d-22-0145.1

Bao, J., & Stevens, B. (2021). The elements of the thermodynamic structure of the tropical atmosphere. *Journal of the Meteorological Society of Japan. Ser. II*, *99*(6), 1483–1499. https://doi.org/10.2151/jmsj.2021-072

Barsugli, J. J., & Sardeshmukh, P. D. (2002). Global atmospheric sensitivity to tropical SST anomalies throughout the indo-Pacific basin. *Journal of Climate*, *15*(23), 3427–3442. https://doi.org/10.1175/1520-0442(2002)015<3427:gastts>2.0.co;2

Betts, A. K. (1982). Saturation point analysis of moist convective overturning. *Journal of the Atmospheric Sciences*, *39*(7), 1484–1505. https://doi.org/10.1175/1520-0469(1982)039<1484:spaomc>2.0.co;2

Bjerknes, J. (1969). Atmospheric teleconnections from the equatorial Pacific. *Monthly Weather Review*, *97*(3), 163–172. https://doi.org/10.1175/1520-0493(1969)097<0163:atftep>2.3.co;2

Bloch-Johnson, J., Rugenstein, M. A., Alessi, M. J., Proistosescu, C., Zhao, M., Zhang, B., et al. (2023). The Green's function model intercomparison project (GFMIP) protocol. *ESS Open Archive*. https://doi.org/10.22541/essoar.167839939.92474288/v1

Bretherton, C. S., & Smolarkiewicz, P. K. (1989). Gravity waves, compensating subsidence and detrainment around cumulus clouds. *Journal of the Atmospheric Sciences*, *46*(6), 740–759. https://doi.org/10.1175/1520-0469(1989)046<0740:gwcsad>2.0.co;2

Ceppi, P., & Gregory, J. M. (2017). Relationship of tropospheric stability to climate sensitivity and Earth's observed radiation budget. *Proceedings of the National Academy of Sciences of the United States of America*, *114*(50), 13126–13131. https://doi.org/10.1073/pnas.1714308114

Charney, J. G. (1963). A note on the large-scale motions in the tropics. *Journal of the Atmospheric Sciences*, *20*(6), 607–609. https://doi.org/10.1175/1520-0469(1963)020<0607:anolsm>2.0.co;2

Dong, Y., Proistosescu, C., Armour, K. C., & Battisti, D. S. (2019). Attributing historical and future evolution of radiative feedbacks to regional warming patterns using a Green's function approach: The preeminence of the western Pacific. *Journal of Climate*, *32*(17), 5471–5491. https://doi.org/10.1175/jcli-d-18-0843.1

Emanuel, K. (2007). Quasi-equilibrium dynamics of the tropical atmosphere. *The Global Circulation of the Atmosphere*, *186*, 218.

Flannaghan, T. J., Fueglistaler, S., Held, I. M., Po-Chedley, S., Wyman, B., & Zhao, M. (2014). Tropical temperature trends in atmospheric general circulation model simulations and the impact of uncertainties in observed SSTs. *Journal of Geophysical Research: Atmospheres*, *119*(23), 13–327. https://doi.org/10.1002/2014jd022365

Forster, P., Storelvmo, T., Armour, K., Collins, W., Dufresne, J. L., Frame, D., et al. (2021). The Earth's energy budget, climate feedbacks, and climate sensitivity. In V. Masson-Delmotte, A. Zhai, S. L. Pirani, C. Connors, S. Péan, N. Berger, et al. (Eds.). *Climate change 2021: The physical science basis. contribution of working group i to the sixth assessment report of the intergovernmental panel on climate change (chap. 7)*. Cambridge University Press.

Fueglistaler, S. (2019). Observational evidence for two modes of coupling between sea surface temperatures, tropospheric temperature profile, and shortwave cloud radiative effect in the tropics. *Geophysical Research Letters*, *46*(16), 9890–9898. https://doi.org/10.1029/2019gl083990

Fueglistaler, S., Dessler, A., Dunkerton, T., Folkins, I., Fu, Q., & Mote, P. W. (2009). Tropical tropopause layer. *Reviews of Geophysics*, *47*(1), RG1004. https://doi.org/10.1029/2008rg000267

Fueglistaler, S., Radley, C., & Held, I. M. (2015). The distribution of precipitation and the spread in tropical upper tropospheric temperature trends in CMIP5/AMIP simulations. *Geophysical Research Letters*, *42*(14), 6000–6007. https://doi.org/10.1002/2015gl064966

Gill, A. E. (1980). Some simple solutions for heat-induced tropical circulation. *Quarterly Journal of the Royal Meteorological Society*, *106*(449), 447–462. https://doi.org/10.1002/qj.49710644905

Held, I. M., & Shell, K. M. (2012). Using relative humidity as a state variable in climate feedback analysis. *Journal of Climate*, *25*(8), 2578–2582. https://doi.org/10.1175/JCLI-D-11-00721.1

Hoerling, M. P., Kumar, A., & Xu, T. (2001). Robustness of the nonlinear climate response to ENSO's extreme phases. *Journal of Climate*, *14*(6), 1277–1293. https://doi.org/10.1175/1520-0442(2001)014<1277:rotncr>2.0.co;2

Hoerling, M. P., Kumar, A., & Zhong, M. (1997). El Niño, La Niña, and the nonlinearity of their teleconnections. *Journal of Climate*, *10*(8), 1769–1786. https://doi.org/10.1175/1520-0442(1997)010<1769:enolna>2.0.co;2

Jenney, A. M., Randall, D. A., & Branson, M. D. (2020). Understanding the response of tropical ascent to warming using an energy balance framework. *Journal of Advances in Modeling Earth Systems*, *12*(6), e2020MS002056. https://doi.org/10.1029/2020MS002056

Johnson, N. C., & Kosaka, Y. (2016). The impact of eastern equatorial Pacific convection on the diversity of boreal winter El Niño teleconnection patterns. *Climate Dynamics*, *47*(12), 3737–3765. https://doi.org/10.1007/s00382-016-3039-1

Johnson, N. C., & Xie, S.-P. (2010). Changes in the sea surface temperature threshold for tropical convection. *Nature Geoscience*, *3*(12), 842–845. https://doi.org/10.1038/ngeo1008

Knutti, R., Rugenstein, M. A., & Hegerl, G. C. (2017). Beyond equilibrium climate sensitivity. *Nature Geoscience*, *10*(10), 727–736. https://doi.org/10.1038/ngeo3017

Koshiro, T., Kawai, H., & Noda, A. T. (2022). Estimated cloud-top entrainment index explains positive low-cloud-cover feedback. *Proceedings of the National Academy of Sciences of the United States of America*, *119*(29), e2200635119. https://doi.org/10.1073/pnas.2200635119

Li, W., & Forest, C. E. (2014). Estimating the sensitivity of the atmospheric teleconnection patterns to SST anomalies using a linear statistical method. *Journal of Climate*, *27*(24), 9065–9081. https://doi.org/10.1175/jcli-d-14-00231.1

Mackie, A., Brindley, H. E., & Palmer, P. I. (2021). Contrasting observed atmospheric responses to tropical sea surface temperature warming patterns. *Journal of Geophysical Research: Atmospheres*, *126*(7), e2020JD033564. https://doi.org/10.1029/2020jd033564

Neale, R. B., & Hoskins, B. J. (2000). A standard test for AGCMS including their physical parametrizations: I: The proposal. *Atmospheric Science Letters*, *1*(2), 101–107. https://doi.org/10.1006/asle.2000.0019

Neelin, J. D., & Held, I. M. (1987). Modeling tropical convergence based on the moist static energy budget. *Monthly Weather Review*, *115*(1), 3–12. https://doi.org/10.1175/1520-0493(1987)115<0003:mtcbot>2.0.co;2

Otto, A., Otto, F. E., Boucher, O., Church, J., Hegerl, G., Forster, P. M., et al. (2013). Energy budget constraints on climate response. *Nature Geoscience*, *6*(6), 415–416. https://doi.org/10.1038/ngeo1836

Park, S., & Leovy, C. B. (2004). Marine low-cloud anomalies associated with ENSO. *Journal of Climate*, *17*(17), 3448–3469. https://doi.org/10.1175/1520-0442(2004)017<3448:mlaawe>2.0.co;2

Pierrehumbert, R. T. (1995). Thermostats, radiator fins, and the local runaway greenhouse. *Journal of the Atmospheric Sciences*, *52*(10), 1784–1806. https://doi.org/10.1175/1520-0469(1995)052<1784:trfatl>2.0.co;2

Pincus, R., & Stevens, B. (2013). Paths to accuracy for radiation parameterizations in atmospheric models. *Journal of Advances in Modeling Earth Systems*, *5*(2), 225–233. https://doi.org/10.1002/jame.20027

Raymond, D. J. (1995). Regulation of moist convection over the west Pacific warm pool. *Journal of the Atmospheric Sciences*, *52*(22), 3945–3959. https://doi.org/10.1175/1520-0469(1995)052<3945:romcot>2.0.co;2

Riley, K. F., Hobson, M. P., & Bence, S. J. (1999). *Mathematical methods for physics and engineering*. American Association of Physics Teachers.

Rugenstein, M., Bloch-Johnson, J., Gregory, J., Andrews, T., Mauritsen, T., Li, C., et al. (2020). Equilibrium climate sensitivity estimated by equilibrating climate models. *Geophysical Research Letters*, *47*(4), e2019GL083898. https://doi.org/10.1029/2019gl083898

Singh, M. S., & O'Gorman, P. A. (2013). Influence of entrainment on the thermal stratification in simulations of radiative-convective equilibrium. *Geophysical Research Letters*, *40*(16), 4398–4403. https://doi.org/10.1002/grl.50796

Stevens, B., Sherwood, S. C., Bony, S., & Webb, M. J. (2016). Prospects for narrowing bounds on Earth's equilibrium climate sensitivity. *Earth's Future*, *4*(11), 512–522. https://doi.org/10.1002/2016ef000376

Sundqvist, H., Berge, E., & Kristjánsson, J. E. (1989). Condensation and cloud parameterization studies with a mesoscale numerical weather prediction model. *Monthly Weather Review*, *117*(8), 1641–1657. https://doi.org/10.1175/1520-0493(1989)117<1641:cacpsw>2.0.co;2

Tiedtke, M. (1989). A comprehensive mass flux scheme for cumulus parameterization in large-scale models. *Monthly Weather Review*, *117*(8), 1779–1800. https://doi.org/10.1175/1520-0493(1989)117<1779:acmfsf>2.0.co;2

Trenberth, K. E., Stepaniak, D. P., & Caron, J. M. (2002). Interannual variations in the atmospheric heat budget. *Journal of Geophysical Research*, *107*(D8), 4066. https://doi.org/10.1029/2000jd000297

Williams, A. I. L., Stier, P., Dagan, G., & Watson-Parris, D. (2022). Strong control of effective radiative forcing by the spatial pattern of absorbing aerosol. *Nature Climate Change*, *12*(8), 735–742. https://doi.org/10.1038/s41558-022-01415-4

Williams, I. N., & Pierrehumbert, R. T. (2017). Observational evidence against strongly stabilizing tropical cloud feedbacks. *Geophysical Research Letters*, *44*(3), 1503–1510. https://doi.org/10.1002/2016gl072202

Wood, R., & Bretherton, C. S. (2006). On the relationship between stratiform low cloud cover and lower-tropospheric stability. *Journal of Climate*, *19*(24), 6425–6432. https://doi.org/10.1175/jcli3988.1

Xie, S.-P., Deser, C., Vecchi, G. A., Ma, J., Teng, H., & Wittenberg, A. T. (2010). Global warming pattern formation: Sea surface temperature and rainfall. *Journal of Climate*, *23*(4), 966–986. https://doi.org/10.1175/2009jcli3329.1

Zhang, B., Zhao, M., & Tan, Z. (2022). Using a Green's function approach to diagnose the pattern effect in GFDL AM4 and CM4. *Journal of Climate*, *1–41*(4), 1105–1124. https://doi.org/10.1175/JCLI-D-22-0024.1

Zhang, C. (1993). Large-scale variability of atmospheric deep convection in relation to sea surface temperature in the tropics. *Journal of Climate*, *6*(10), 1898–1913. https://doi.org/10.1175/1520-0442(1993)006<1898:lsvoad>2.0.co;2

Zhang, Y., & Fueglistaler, S. (2020). How tropical convection couples high moist static energy over land and ocean. *Geophysical Research Letters*, *47*(2), e2019GL086387. https://doi.org/10.1029/2019gl086387

Zhao, M., Held, I. M., Lin, S.-J., & Vecchi, G. A. (2009). Simulations of global hurricane climatology, interannual variability, and response to global warming using a 50-km resolution GCM. *Journal of Climate*, *22*(24), 6653–6678. https://doi.org/10.1175/2009jcli3049.1

Zhou, C., Zelinka, M. D., & Klein, S. A. (2016). Impact of decadal cloud variations on the Earth's energy budget. *Nature Geoscience*, *9*(12), 871–874. https://doi.org/10.1038/ngeo2828

Zhou, C., Zelinka, M. D., & Klein, S. A. (2017). Analyzing the dependence of global cloud feedback on the spatial pattern of sea surface temperature change with a Green's function approach. *Journal of Advances in Modeling Earth Systems*, *9*(5), 2174–2189. https://doi.org/10.1002/2017ms001096